7.4 Momentum Integral Methods

Historically similarity and other AFD methods used for idealized flows and momentum integral methods for practical applications, including pressure gradients, but failure 3D methods motivated 3D BL theory which quickly progressed to modern day CFD.

Momentum integral equation, which is valid for both laminar and turbulent flow:

$$\int_{y=0}^{\infty} (\text{steady flow BL equation } + (u-U)\text{continuity})\, dy$$

$$\underbrace{\frac{\tau_w}{\rho U^2} = \frac{1}{2} C_f}_{} = \frac{d\theta}{dx} + (2+H)\frac{\theta}{U}\frac{dU}{dx}$$

For flat plate equation → $\frac{dU}{dx} = 0$

$$\theta = \int_0^{\delta} \frac{u}{U}\left(1 - \frac{u}{U}\right) dy$$

$$\delta^* = \int_0^{\delta} \left(1 - \frac{u}{U}\right) dy$$

$$H = \frac{\delta^*}{\theta}$$

Momentum: $uu_x + vu_y = -\frac{\partial}{\partial x}\left(\frac{p}{\rho}\right) + \frac{1}{\rho}\frac{\partial \tau}{\partial y}$ where $\tau = \mu \frac{\partial u}{\partial y}$

The pressure gradient evaluated form the outer potential flow using Bernoulli equation.

$$p + \frac{1}{2}\rho U^2 = \text{constant}$$

$$p_x + \frac{1}{2}\rho 2 U U_x = 0$$

$$-p_x/\rho = U U_x$$

$$(u-U)\underbrace{(u_x+v_y)}_{Continuity}=uu_x+uv_y-Uu_x-Uv_y$$

$$\underbrace{uu_x+vu_y-UU_x-\frac{1}{\rho}\tau_y}_{0}+\underbrace{uu_x+uv_y-Uu_x-Uv_y}_{0}=0$$

$$-\frac{1}{\rho}\tau_y=-2uu_x-vu_y+UU_x-uv_y+Uu_x+Uv_y$$

$$=\frac{\partial}{\partial x}(uU-u^2)+(U-u)U_x+\frac{\partial}{\partial y}(vU-vu)$$

$$\int_0^\infty -\frac{1}{\rho}\tau_y dy=-(\overset{0}{\tau_\infty}-\tau_w)/\rho=\frac{\partial}{\partial x}\int_0^\infty u(U-u)dy+U_x\int_0^\infty(U-u)dy+\overset{0}{(vU-vu)}\Big|_0^\infty$$

$$\frac{\tau_w}{\rho}=\frac{\partial}{\partial x}\left[U^2\int_0^\infty\frac{u}{U}\left(1-\frac{u}{U}\right)dy\right]+U_xU\int_0^\infty\left(1-\frac{u}{U}\right)dy$$

$$=U^2\theta_x+2UU_x\theta+UU_x\delta^*$$

$$\frac{\tau_w}{\rho U^2}=\frac{1}{2}C_f=\theta_x+(2\theta+\delta^*)\frac{1}{U}\frac{dU}{dx}$$

$$\frac{C_f}{2}=\frac{d\theta}{dx}+(2+H)\frac{\theta}{U}U_x$$

Methods Solution Momentum Integral Equation

Historically two approaches:

(1) One parameter velocity profiles
(2) Empirical correlations: Thwaites method

(1) Karman-Pohlhausen Method

1. $u(x,y) = U(x) f[y/\delta, \Lambda(x)]$ guess form velocity profile

   $u/U = 2\eta - 2\eta^3 + \eta^4 + \frac{\Lambda}{6}[\eta(1-\eta)^3]$ $\quad \eta = y/\delta$

2. use 5 BC for u/U $\quad \Lambda = \frac{\delta^2}{\nu} U_x$ = Pohlhausen parameter
3. compute: $\theta, \delta^*, H, \tau_w$
4. Substitute momentum integral equation for 1st order ODE $\delta(x)$
5. with $\delta(x)$ known all variables also known

Accuracy not as good Thwaites method

Issues:

Recall using quadratic guessed profile flat plate velocity profile only 10% accuracy.

Accuracy depends type of guessed profile.

TABLE 4-1

Boundary-layer predictions from five piecewise analytic profiles with their errors relative to the classic Blasius values

	$\frac{u}{U} = F(\xi)$	$\eta^* = \frac{\delta^*}{\delta}$	$\theta^* = \frac{\theta}{\delta}$	$H = \frac{\delta^*}{\theta}$	$\frac{\delta}{x}\sqrt{Re_x}$	$C_f\sqrt{Re_x}$	$\frac{\delta^*}{x}\sqrt{Re_x}$	L_2 error
1	$2\xi - \xi^2$	0.333 3.1%	0.133 0.25%	2.500 3.5%	5.477 9.5%	0.730 10%	1.826 6.1%	0.020
2	$\frac{3}{2}\xi - \frac{1}{2}\xi^3$	0.375 9.0%	0.139 4.7%	2.692 4.0%	4.641 7.2%	0.646 2.6%	1.740 1.1%	0.034
3	$2\xi - 2\xi^3 + \xi^4$	0.300 13%	0.118 12%	2.554 1.4%	5.836 17%	0.685 3.2%	1.751 1.8%	0.054
4	$\sin\left(\frac{1}{2}\pi\xi\right)$	0.363 5.6%	0.137 2.7%	2.660 2.7%	4.795 4.1%	0.655 1.3%	1.743 1.3%	0.021
5	$\frac{3}{2}\xi - \xi^3 + \frac{1}{2}\xi^4$	0.350 1.7%	0.134 0.52%	2.618 1.1%	4.993 0.13%	0.668 0.53%	1.748 1.6%	0.008
	Blasius (1908)	0.344	0.133	2.59	5	0.664	1.72	n/a

$L_2 = \left[\int_0^1 (F - F_{Blasius})^2 d\eta\right]$

1, 2, 3 Pohlhausen (1921)
4 Schlichting (1979)
5 Majdalani & Xuan (2020)

Pohlhausen paradox: increasing order, i.e., # BC profile can satisfy does not improve accuracy

BC: $u(x,0) = 0$ 1 no slip
$u(x,\delta) = U$ 2 match
$u_y(x,\delta) = 0$ 3 smooth merge U
$\mu u_{yy}(x,0) = p_x$ 4 correct balance momentum y=0
$u_{yy}(x,\delta) = 0$ 5 $\mu \frac{\partial}{\partial y}\tau_y = 0$ zero shear stress at δ

However, the Blasius profile does not in fact satisfy all these conditions!

Note 1 satisfies BC 1-3 & 2-5 satisfy BC 1-4 but only 3 satisfies BC 1-5 & largest L_2 error

BC's true at $y \to \infty$ but not true $y = \delta$ where $u_{yy}\big|_{\delta,\ \text{Blasius}} = -.7085$

Also higher initial slope $F'(0)$

Other differences such as $F(1)$ & $F'(1)$

TABLE 4-2

Endpoint properties of the piecewise analytic velocity profiles and their corresponding Blasius values

$\frac{u}{U} = F(\xi)$	$F(0)$	$F'(0)$	$F''(0)$	$F(1)$	$F'(1)$	$F''(1)$
$2\xi - \xi^2$	0	2.000	−2	1.000	0	−2.000
$\frac{3}{2}\xi - \frac{1}{2}\xi^3$	0	1.500	0	1.000	0	−3.000
$2\xi - 2\xi^3 + \xi^4$	0	2.000	0	1.000	0	0.000
$\sin\left(\frac{1}{2}\pi\xi\right)$	0	1.571	0	1.000	0	−2.467
$\frac{5}{3}\xi - \xi^3 + \frac{1}{3}\xi^4$	0	1.667	0	1.000	0	−2.000
Blasius (1908)	0	1.630	0	0.990	0.0904	−0.709

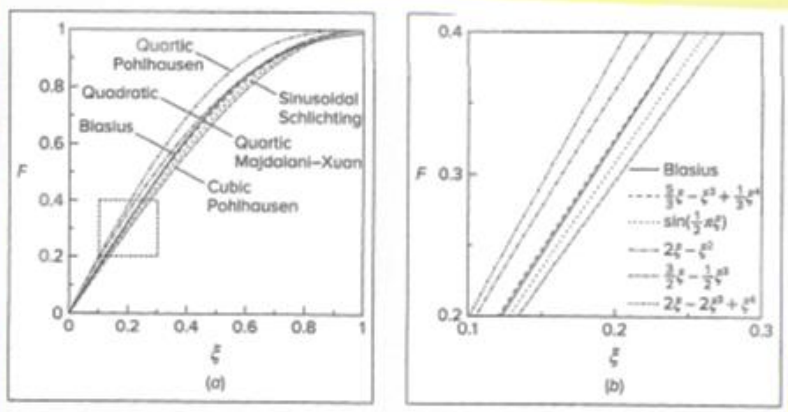

FIGURE 4-5
Comparison of five analytic approximations to the Blasius solution (solid line) including Pohlhausen's quadratic, cubic, and quartic polynomials (chained lines) as well as Schlichting's sinusoidal (dotted) and Majdalani–Xuan's quartic (dashed) profiles across (*a*) the boundary layer and (*b*) a designated quadrant where individual deviations from the Blasius curve are magnified.

Presumably these differences compounded for $p_x \neq 0$.

Thwaites Method (1949)

Pressure gradient parameter $\lambda = \frac{\theta^2}{\nu}\frac{dU}{dx} = (\frac{\theta}{\delta})^2\Lambda$ where $\Lambda = \frac{\delta^2}{\nu}\frac{dU}{dx} = -p_x\frac{\delta^2}{\mu U}$ is the Pohlhausen parameter.

Multiply momentum integral equation by $\frac{U\theta}{\nu}$

$$\frac{\tau_w\theta}{\mu U} = \frac{U\theta}{\nu}\frac{d\theta}{dx} + \frac{\theta^2}{\nu}\frac{dU}{dx}(2+H)$$

The equation is dimensionless and, LHS and H can be correlated with λ as shear and shape-factor correlations:

$$\frac{\tau_w\theta}{\mu U} = S(\lambda) = (\lambda + 0.09)^{0.62}$$

$$H = \delta^*/\theta = H(\lambda) = \sum_{i=0}^{5} a_i(0.25-\lambda)^i$$

a_i = (2, 4.14, -83.5, 854, -3337, 4576)

Note

$$\frac{U\theta}{\nu}\frac{d\theta}{dx} = \frac{1}{2}U\frac{d}{dx}\left(\frac{\theta^2}{\nu}\right)$$

Substitute above into momentum integral equation.

$$S(\lambda) = \frac{1}{2}U\frac{d}{dx}\left(\frac{\theta^2}{\nu}\right) + \lambda(2+H)$$

$$U\frac{d(\lambda/U_x)}{dx} = 2[S - \lambda(2+H)\lambda] = F(\lambda)$$

$F(\lambda) = 0.45 - 6\lambda$ based on AFD and EFD

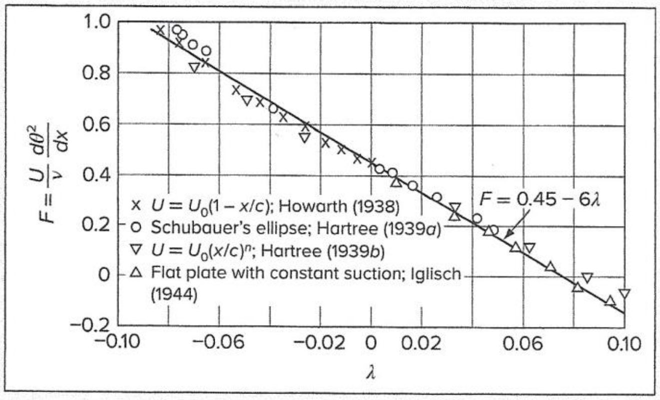

FIGURE 4-27
Empirical correlation of the boundary-layer function in Eq. (4-156). [*After Thwaites (1949)*.]

Define $z = \frac{\theta^2}{\nu}$ so that $\lambda = z\frac{dU}{dx}$

$$U\frac{dz}{dx} = 0.45 - 6\lambda = 0.45 - 6z\frac{dU}{dx}$$

$$U\frac{dz}{dx} + 6z\frac{dU}{dx} = 0.45$$

$$\frac{1}{U^5}\frac{d}{dx}(zU^6) = U\frac{dz}{dx} + 6z\frac{dU}{dx} = 0.45$$

$$d(zU^6) = 0.45U^5dx$$

$$zU^6 = 0.45\int_0^x U^5dx + C$$

$$\Rightarrow \theta^2 = \theta_0^2 + \frac{0.45\nu}{U^6}\int_0^x U^5dx$$

$\theta_0(x = 0) = 0$ and U(x) known from potential flow solution.

Complete solution:

$$\lambda = \lambda(\theta) = \frac{\theta^2}{\nu}\frac{dU}{dx}$$

$$\frac{\tau_w \theta}{\mu U} = S(\lambda)$$

$$\delta^* = \theta H(\lambda)$$

Accuracy: mild p_x $\pm 5\%$ and strong adverse p_x (τ_w near 0) $\pm 15\%$

TABLE 4-8

Shear and shape functions correlated by Thwaites (1949)

λ	$H(\lambda)$	$S(\lambda)$	λ	$H(\lambda)$	$S(\lambda)$
+0.25	2.00	0.500	−0.056	2.94	0.122
0.20	2.07	0.463	−0.060	2.99	0.113
0.14	2.18	0.404	−0.064	3.04	0.104
0.12	2.23	0.382	−0.068	3.09	0.095
0.10	2.28	0.359	−0.072	3.15	0.085
+0.080	2.34	0.333	−0.076	3.22	0.072
0.064	2.39	0.313	−0.080	3.30	0.056
0.048	2.44	0.291	−0.084	3.39	0.038
0.032	2.49	0.268	−0.086	3.44	0.027
0.016	2.55	0.244	−0.088	3.49	0.015
0.0	2.61	0.220	−0.090	3.55 (Separation)	0.000
−0.016	2.67	0.195			
−0.032	2.75	0.168			
−0.040	2.81	0.153			
−0.048	2.87	0.138			
−0.052	2.90	0.130			

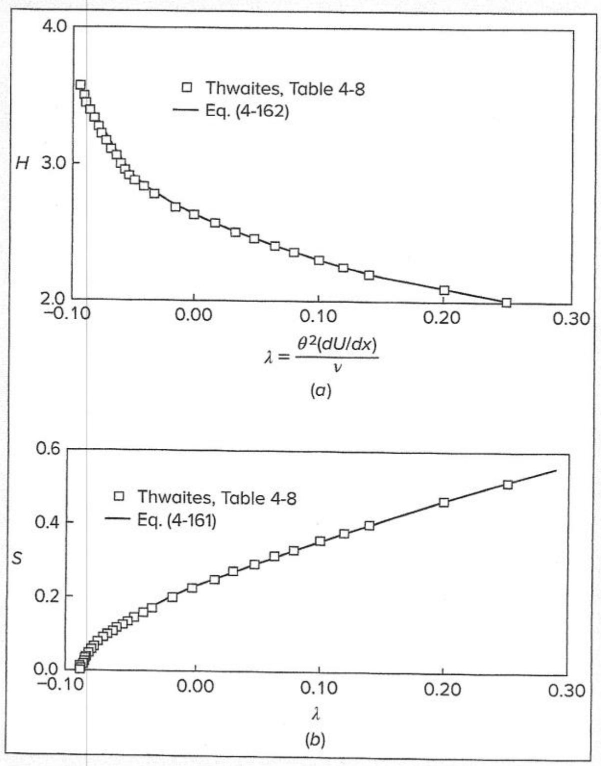

FIGURE 4-28
The laminar boundary-layer correlated functions by Thwaites (1949): (*a*) shape factor; (*b*) shear stress with curve fits.

Separation predicted within 4%; however, large scale separation causes viscous/inviscid interaction and alters imposed external U(x) and $p_x(x)$

TABLE 4-9
Laminar-separation-point prediction by Thwaites' method

$U(x)$	x_{sep} (exact)	Thwaites x_{sep}	Thwaites Error [%]
Howarth (1938)			
$1 - x$	0.120	0.123	+2.5
Tani (1949)			
$1 - x^2$	0.271	0.268	−1.1
$1 - x^4$	0.462	0.449	−2.8
$1 - x^8$	0.640	0.621	−3.0
Terrill (1960)			
$\sin(x)$	1.823	1.800	−1.3
Curle (1958)			
$x - x^3$	0.655	0.648	−1.1
Görtler (1957)			
$\cos(x)$	0.389	0.384	−1.3
$(1 - x)^{1/2}$	0.218	0.221	+1.3
$(1 - x)^2$	0.0637	0.0652	+2.4
$(1 + x)^{-1}$	0.151	0.158	+4.6
$(1 + x)^{-2}$	0.0713	0.0739	+3.6

Pohlhausen Velocity Profile:

$\frac{u}{U} = f(\eta) = a\eta + b\eta^2 + c\eta^3 + d\eta^4$ with $\eta = \frac{y}{\delta}$

a, b, c, d determined from boundary conditions:

1) $y = 0 \rightarrow u = 0,\ u_{yy} = -\frac{U}{\nu}U_x$
2) $y = \delta \rightarrow u = U,\ u_y = 0,\ u_{yy} = 0$

$\rightarrow \frac{u}{U} = F(\eta) + \Lambda G(\eta),\ -12 \le \Lambda \le 12 \quad \Lambda = \frac{\delta^2}{\nu}\frac{dU}{dx} = -p_x\frac{\delta^2}{\mu U}$

separation (experiment: $\Lambda_{separation}$ = -5)

$F(\eta) = 2\eta - 2\eta^3 + \eta^4$

$G(\eta) = \frac{\eta}{6}(1-\eta)^3$

$\lambda = \lambda(\Lambda) = \left(\frac{37}{315} - \frac{\Lambda}{945} + \frac{\Lambda^2}{9072}\right)\Lambda$

Profiles are realistic, except near separation. In guessed profile methods u/U directly used to solve momentum integral equation numerically, but accuracy not as good as empirical correlation methods; therefore, use Thwaites method to get λ, etc., and then use λ to get Λ and plot u/U.

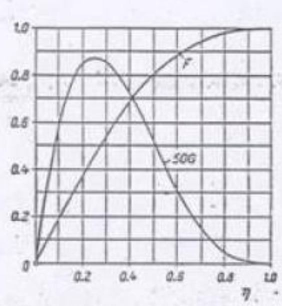

Fig. 10.3. The functions $F(\eta)$ and $G(\eta)$ for the velocity distribution in the boundary layer from eqns. (10.22) and (10.23)

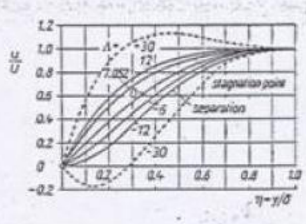

Fig. 10.4. The one-parameter family of velocity profiles from eqn. (10.22)

Howarth linearly decelerating flow (example of exact solution of steady state 2D boundary layer)

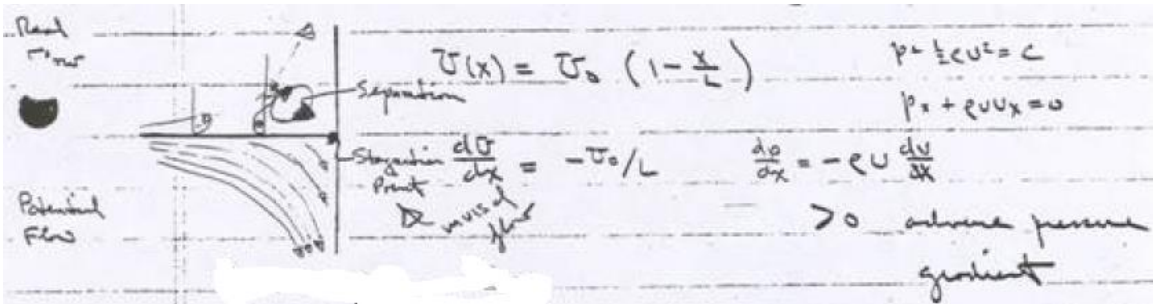

Howarth proposed a linearly decelerating external velocity distribution $U(x) = U_0\left(1 - \frac{x}{L}\right)$ as a theoretical model for laminar boundary layer study. Use Thwaites's method to compute:

a) X_{sep}
b) $C_f\left(\frac{x}{L} = 0.1\right)$

Note $U_x = -U_0/L$

Solution

$$\theta^2 = \frac{0.45\nu}{U_0^6\left(1 - \frac{x}{L}\right)^6}\int_0^x U_0^5\left(1 - \frac{x}{L}\right)^5 dx = 0.075\frac{\nu L}{U_0}\left[\left(1 - \frac{x}{L}\right)^{-6} - 1\right]$$

can be evaluated for given L, Re_L

$$\lambda = \frac{\theta^2}{\nu}\frac{dU}{dx} = -0.075\left[\left(1 - \frac{x}{L}\right)^{-6} - 1\right]$$

$$\lambda_{sep} = -0.09 \Rightarrow \frac{X_{sep}}{L} = 0.123$$

3% higher than exact solution =0.1199

$C_f\left(\frac{x}{L}=0.1\right)$ → i.e. just before separation

$$\lambda = -0.0661$$

$$S(\lambda) = 0.099 = \frac{1}{2}C_f Re_\theta$$

$$C_f = \frac{2(0.099)}{Re_\theta}$$

Compute Re_θ in terms if Re_L

$$\theta^2 = 0.075\frac{\nu L}{U_0}\left[(1-0.1)^{-6}-1\right] = 0.0661\frac{\vartheta L}{U_0}$$

$$\frac{\theta^2}{L^2} = 0.0661\frac{\nu L}{U_0} = \frac{0.0661}{\mathrm{Re}_L}$$

$$\frac{\theta}{L} = \frac{0.257}{\mathrm{Re}_L^{1/2}}$$

$$\mathrm{Re}_\theta = \frac{\theta}{L}\mathrm{Re}_L = 0.257\,\mathrm{Re}_L^{1/2}$$

$$C_f = \frac{2(0.099)}{0.257}\mathrm{Re}_L^{-1/2} = 0.77\,\mathrm{Re}_L^{-1/2}$$

To complete solution must specify Re_L

Consider the complex potential

$$F(z)=\frac{a}{2}z^2=\frac{a}{2}r^2e^{2i\theta}$$

$$\varphi=\mathrm{Re}[F(z)]=\frac{a}{2}r^2\cos 2\theta$$

$$\psi=\mathrm{Im}[F(z)]=\frac{a}{2}r^2\sin 2\theta$$

Orthogonal rectangular hyperbolas

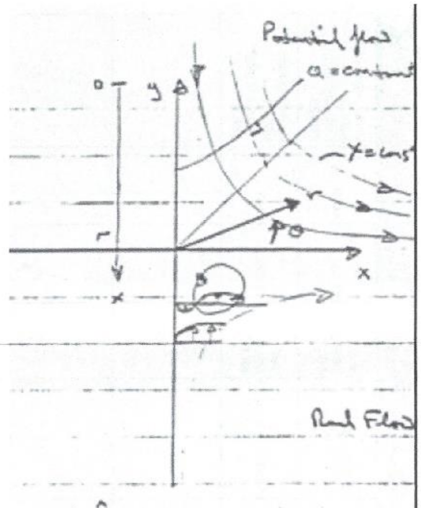

φ: asymptotes y = ± x

ψ : asymptotes x=0, y=0

$\hat{e}_r = \cos\theta\,\hat{i} + \sin\theta\,\hat{j}$

$\hat{e}_\theta = -\sin\theta\,\hat{i} + \cos\theta\,\hat{j}$

$$\underline{V}=\nabla\varphi=\varphi_r\hat{e}_r+\frac{1}{r}\varphi_\theta\hat{e}_\theta$$

$$v_r=ar\cos 2\theta$$

$$v_\theta=-ar\sin 2\theta$$

$\frac{\pi}{2}\le\theta\le 0$ (flow direction as shown)

$$\underline{V}=v_r\left(\cos\theta\hat{i}+\sin\theta\hat{j}\right)+v_\theta\left(-\sin\theta\hat{i}+\cos\theta\hat{j}\right)=$$

$$\left(v_r\cos\theta-v_\theta\sin\theta\right)\hat{i}+\left(v_r\sin\theta+v_\theta\cos\theta\right)\hat{j}$$

Potential flow slips along surface: (consider $\theta=90^\circ$)

1) determine a such that $v_r=U_0$ at r=L, $\theta=90^\circ$

$v_r=aL\cos(2\times 90)=U_0\Rightarrow aL=-U_0$, i.e. $a=-\frac{U_0}{L}$

2) let $U(x)=v_r$ at x=L-r:

$\Rightarrow v_r=a(L-x)\cos(2\times 90)=U(x)$

$Or:\ U(x)=-a(L-x)=\frac{U_0}{L}(L-x)=U_0(1-\frac{x}{L})$

$\psi = Bxy \quad B = U/L$

$u = Bx = \psi_y$

$v = -By = -\psi_x$

$p+\frac{1}{2}\rho(u^2+v^2)=C$

$p+\frac{1}{2}\rho B^2(x^2+y^2)=C$

$p(0,0)=C=p_0$

$p=p_0-\frac{1}{2}\rho\frac{U^2}{L^2}(x^2+y^2)$

$p_x=-\rho\frac{U^2}{L^2}x$

$p_y=-\rho\frac{U^2}{L^2}y$

$U_x=-\frac{U_0}{L}$

$p+\frac{1}{2}\rho U^2=C$

$p_x+\rho UU_x=0$

$p_x=-\rho UU_x=-\rho U_0(1-\frac{x}{L})(-\frac{U_0}{L})=\rho\frac{U_0^2}{L}(1-\frac{x}{L})$

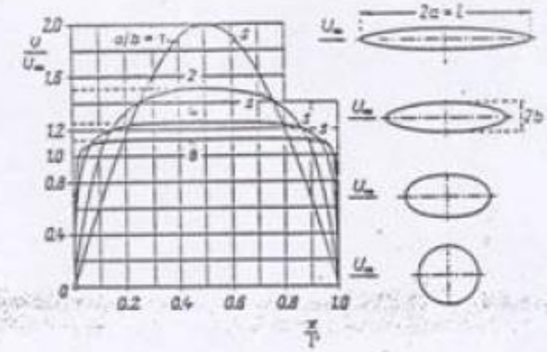

Fig. 10.9. Potential velocity distribution function on elliptical cylinders of slenderness $a/b = 1, 2, 4, 8$, the direction of the stream being parallel to the major axis
S = position of point of separation

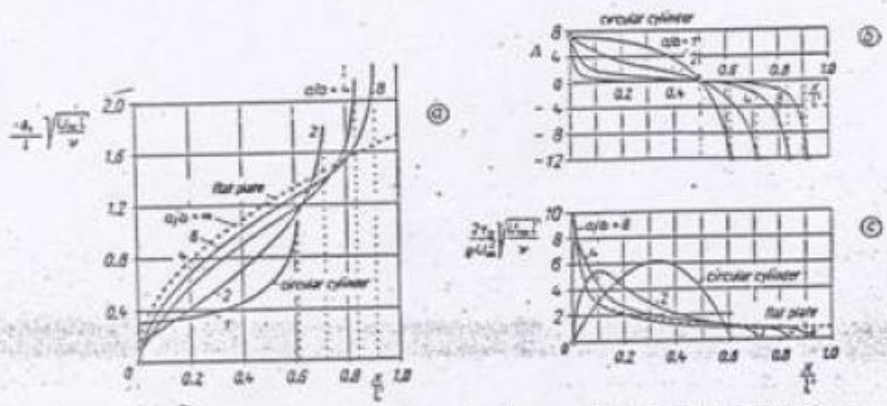

Fig. 10.10. Results of the calculation of boundary layers on elliptical cylinders of slenderness $a/b = 1, 2, 4, 8$, Fig. 10.9. a) displacement thickness of the boundary layer, b) shape factor c) shearing stress at the wall, $2\,l'$ = circumference of the ellipse; $a/b = 1$ circular cylinder; $a/b = \infty$ flat plate

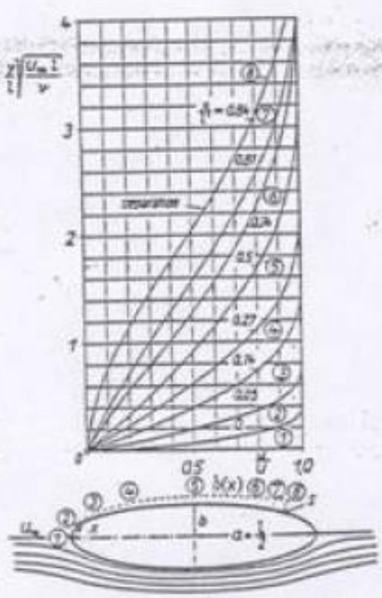

Fig. 10.11. Velocity profiles in the laminar boundary layer on an elliptical cylinder. Ratio of axes $a/b = 4$

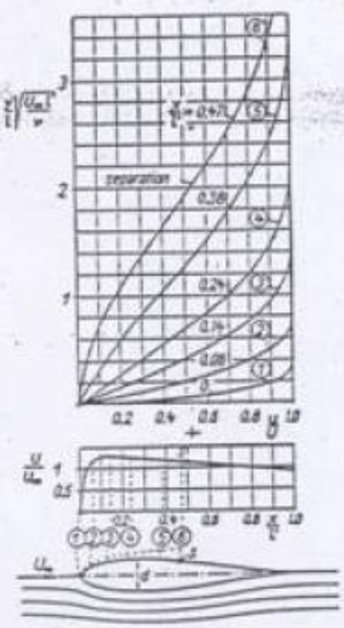

Fig. 10.12. Velocity profiles in the laminar boundary layer and potential velocity function for a Zhukovskii aerofoil J 015 of thickness ratio $d/l = 0{\cdot}15$ at an angle of incidence $\alpha = 0$

Refer back to Table 4-6 (Lec 26) with regard to relative performance of integral methods

3-D Integral methods

Momentum integral methods perform well (i.e. compare well with experimental data) for a large class of both laminar and turbulent 2D flows. However, for ***3D flows they do not***, primarily due to the inability of correlating the crossflow velocity components.

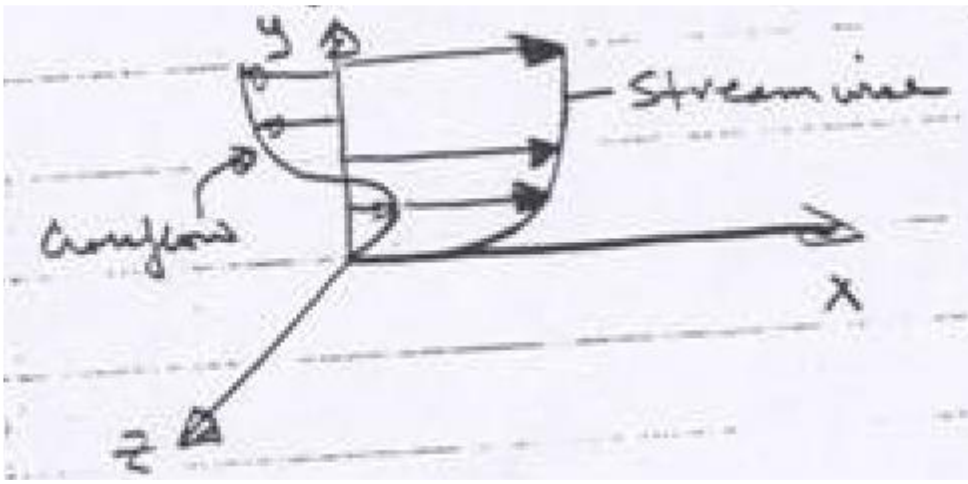

The cross flow is driven by $\frac{\partial p}{\partial z}$, which is imposed on BL from the outer potential flow U(x,z).

3-D boundary layer equations

$$u_x + v_y + w_z = 0;$$
$$uu_x + vu_y + wu_z = -\frac{\partial}{\partial x}(p/\rho) + \nu u_{yy} - \frac{\partial}{\partial y}(\overline{u'v'})$$
$$uw_x + vw_y + ww_z = -\frac{\partial}{\partial z}(p/\rho) + \nu w_{yy} - \frac{\partial}{\partial y}(\overline{v'w'})$$
$$+ \quad \text{closure equations}$$

Differential methods have been developed for this reason as well as for extensions to more complex and non-thin boundary layer flows.